UC Berkeley
UC Berkeley Previously Published Works

Title
Magnetic multilayer edges in Bernal-stacked hexagonal boron nitride

Permalink
https://escholarship.org/uc/item/2cc1t4bb

Journal
Physical Review B, 102(15)

ISSN
2469-9950

Authors
Dogan, Mehmet
Cohen, Marvin L

Publication Date
2020-10-01

DOI
10.1103/physrevb.102.155419

Peer reviewed

Magnetic Multilayer Edges in Bernal-Stacked Hexagonal Boron Nitride

Mehmet Dogan[1,2] and Marvin L. Cohen[1,2]

[1]*Department of Physics, University of California, Berkeley, California 94720, USA*
[2]*Materials Sciences Division, Lawrence Berkeley National Laboratory, Berkeley, California 94720, USA*

Single-layer h-BN is known to have edges with unique magnetism, however, in the commonly fabricated multilayer AA′-h-BN, edge relaxations occur that create interlayer bonds and eliminate the unpaired electrons at the edge. Recently, a robust method of growing the unconventional Bernal-stacked h-BN (AB-h-BN) has been reported. Here, we use theoretical approaches to investigate the nitrogen-terminated zigzag edges in AB-h-BN that can be formed in a controlled fashion using a high-energy electron beam. We find that these "open" edges remain intact in bilayer and multilayer AB-h-BN, enabling researchers potentially to investigate these edge states experimentally. We also investigate the thermodynamics of the spin configurations at the edge by constructing a lattice model that is based on parameters extracted from a set of first-principles calculations. We find that the edge spins in neighboring layers interact very weakly, resulting in a sequence of independent spin chains in multilayer samples. By solving this model using Monte Carlo simulations, we can determine nm-scale correlation lengths at liquid-N_2 temperatures and lower. At low temperatures, these edges may be utilized in magnetoresistance and spintronics applications.

I. INTRODUCTION

Among the many novel research avenues that have been created by two-dimensional (2D) materials, an important one is that their terminations provide a robust platform to study one-dimensional (1D) systems. For example, by terminating a sheet of a 2D material by two parallel edges separated by a small distance, nanoribbons are formed. Similarly, nanoflakes are made by fabricating three or more edges which fully surround the nanosheet to obtain a finite (0D) system. These have led to a new field of research by allowing the study of many physical phenomena in reduced-dimensional systems [1]. In a similar vein, fabricating nanopores in 2D materials have been an important field of research that touches upon molecular sieving, metamaterials and quantum emission [2–5]. Nanopores are also made up of edges, but are in a sense the "opposite" of nanoflakes. In addition to engineering these edges to fabricate nanoribbons, nanoflakes and nanopores, edges inevitably occur in real nanosheets and affect experimental observations. Therefore, it is important to understand the properties of edges themselves, which can be done by considering a nanoribbon with a large enough width. Such a system can be interpreted as a collection of two parallel edges and an interior region where the edges can be treated independently, and the interior can be treated like an infinite sheet. In this study, we investigate the properties of the most commonly observed edge type in single-layer hexagonal boron nitride (h-BN) as well as its interaction with neighboring layers and edges, which is largely determined by the stacking sequence.

Stacking the layers of h-BN in different ways yields different material properties without altering the structure within each layer [6–9]. The trivial stacking sequence [Figure 1(a)] is named the AA stacking, where there is no in-plane shift or rotation between consecutive lay-
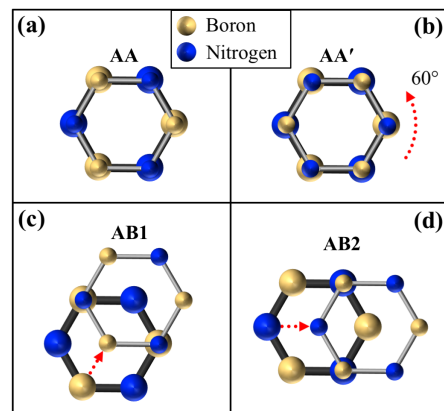

Figure 1. Four high-symmetry stacking sequences of h-BN considered in this study. (a) The AA stacking sequence which has not been observed experimentally. (b) The commonly observed AA′ stacking sequence. (c,d) Two ways of constructing the AB stacking sequence of h-BN. These two ways are physically equivalent but geometrically distinct, and are distinguished so that the top and the bottom layers can be treated separately.

ers. When this stacking is repeated to form bulk h-BN, columns of B atoms and columns of N atoms in the out-of-plane direction are created. Although this high-energy stacking sequence has not been experimentally observed, we include it in our study as a reference, and find that it has an interlayer distance of 3.64 Å. Common synthesis methods yield a bilayer stacking sequence [Figure 1(b)], named the AA′ stacking, where there is a 60° rotation between consecutive layers, which results in columns of alternating B and N atoms in the bulk [10]. An alternative stacking sequence, where there is a shift but no rotation between consecutive layers [Figure 1(c,d)], named the AB stacking, had been observed in rare cases until recently [11–13]. However, Gilbert *et al.* demonstrated a

robust and reproducible method of growing AB stacked h-BN (AB-h-BN) [9]. Many computed properties of AB-h-BN are similar to those of AA′-h-BN, such as interlayer distance (AB: 3.09 Å vs. AA′: 3.11 Å), indirect band gap (AB: 4.43 eV vs. AA′: 4.41 eV) and dielectric tensor [9]. Therefore the new AB-h-BN can be used interchangeably with AA′-h-BN in many materials applications.

Although an infinite sheet of single-layer h-BN is a wide-gap insulator, computational studies have shown that its edges exhibit a rich collection of electronic and magnetic properties [14–18]. Magnetism that is found on these edges arises from unpaired electrons that occupy dangling sp^2 hybrid orbitals. However, because of the existence of various spin configurations within a small total energy window, a thermodynamic analysis is needed to make predictions at nonzero temperatures. Furthermore, experimental studies aimed at locally probing the electronic structure at the edge are needed to complete our understanding of these systems. The most commonly observed edge type in h-BN is the nitrogen-terminated zigzag edge (N-edge) [10, 19–25], shown in Figure 2. By the application of a high-energy electron beam in a transmission electron microscopy (TEM) chamber, it is possible to fabricate the N-edge almost exclusively among all edge types [9, 26–29]. In this study, we investigate the spin configurations of the N-edge in single-layer h-BN and build a statistical model to make predictions about the magnetic properties of real edges. We then discuss what happens to the N-edge in multilayer h-BN. Because of the lack of relative rotation between the consecutive layers in AB-h-BN, multilayer N-edges can be formed [9, 29], which is not possible in AA′-h-BN because of the 60° rotation between consecutive layers [26]. Additionally, it has been observed that in AA′-h-BN, edge relaxations occur and give rise to covalent bonding between the edge atoms in the neighboring layers [30], which is not the case for AB-h-BN [29].

We note that in AB-h-BN, the two consecutive layers are inequivalent. Specifically, in Figure 1(c), the N atom in the top layer is aligned with the B atom in the bottom layer, whereas the B atom in the top layer is aligned with the hollow site of the bottom layer. Therefore the B (N) atom of the top layer is not in the same physical environment as the B (N) atom of the bottom layer. Given a starting bottom layer, the top layer may be formed in two distinct ways, shown in Figure 1(c,d), which we name AB1 and AB2, respectively. The top layer in AB1 then becomes equivalent to the bottom layer in AB2, and vice versa. So the distinction between these two types within the AB stacking is meaningful when we are considering a well-defined bottom layer and a well-defined top layer, as we will in the discussion below.
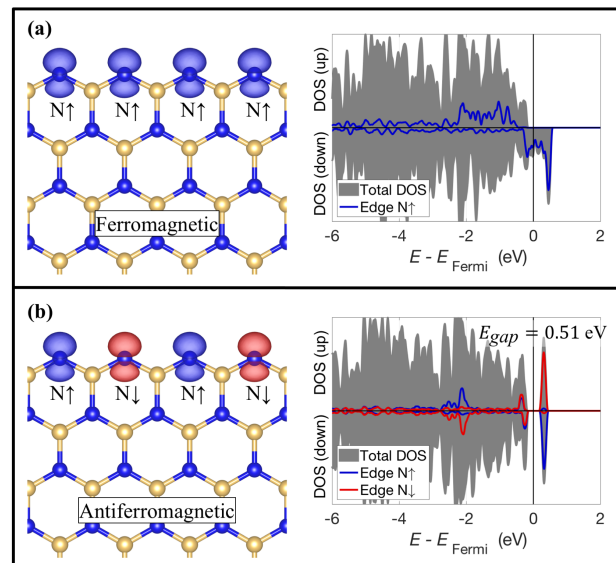

Figure 2. The ferromagnetic (a) and antiferromagnetic (b) N-terminated zigzag edge configurations of the monolayer h-BN. The isosurface plots for magnetization with the isovalue $n_\uparrow - n_\downarrow = \pm 0.02 \ |e|/a_0^3$ are included in the atomic structure pictures. The spin-resolved densities-of-states plots including the projections onto the orbitals of the edge nitrogen atom are also shown.

II. METHODS

We use density functional theory (DFT) in the Perdew–Burke–Ernzerhof generalized gradient approximation (PBE GGA) to conduct our *ab initio* calculations [31]. We employ the QUANTUM ESPRESSO software package with norm-conserving pseudopotentials [32, 33]. We have converged our calculations with respect to the plane-wave energy cutoff for the pseudo Kohn-Sham wavefunctions, which has yielded a value of 80 Ry. For single- and double-layer edge simulations, we use a $12 \times 1 \times 1$ Monkhorst–Pack k-point mesh per unit edge to sample the Brillouin zone [34]. A 1×10 cell is constructed, and ~12 Å of vacuum is placed between the copies of the 1D system along the direction perpendicular to the edge. The dangling bonds at the opposite edge are passivated using hydrogen atoms. We keep the first 4 unit cells (8 atoms) unrelaxed, and relax the remaining 6 unit cells (12 atoms). In order to include the interlayer van der Waals interactions, we include a Grimme-type dispersion correction [35]. All atomic coordinates are relaxed until the forces on all the atoms are less than 10^{-3} Ry/a_0 in all three Cartesian directions, where a_0 is the Bohr radius. A ~14 Å thick vacuum is used between the periodic copies of the slab in the out-of-plane direction to isolate the sheets.

III. RESULTS

A. Open Edges in h-BN

In Figure 2, we present the N-edge of a monolayer h-BN sheet. The ferromagnetic (FM) and antiferromagnetic (AFM) states are presented in Figure 2(a,b), respectively. The isosurface plots for magnetization with the isovalue $n_\uparrow - n_\downarrow = \pm 0.02 \; |e|/a_0^3$ show a spatially localized spin polarization on the dangling sp^2 orbitals on the edge N atoms. Both states are lower in energy than the nonmagnetic state, and the ferromagnetic state is the ground state [Table I]. In both the FM and AFM states, the magnetization per edge N atom is 1 μ_{B}. There is negligible relaxation (< 0.01 Å) at these edges arising from the change in the spin configuration. The spin-resolved densities-of-states (DOS) plots show that the ferromagnetic edge is a half-metal, i.e. the majority spin channel is insulating and the minority spin channel is a metal, which should give rise to a fully spin-polarized edge current and potentially enable spintronic devices such as tunnel junctions, spin filters, diodes and transistors [36–39]. The antiferromagnetic state is a semiconductor with a gap of 0.51 eV. Because the spin configuration and the electronic structure are closely linked, these edges may be useful in metal spintronics as well as semiconductor spintronics applications [36–42]. Our findings on the monolayer h-BN agree well with the existing computational studies [14, 15, 18, 43, 44].

When the bilayer h-BN is formed in the AB stacking, the N-edge remains "open" upon relaxation, *i.e.* no interlayer bonds form. This results in essentially two copies of the monolayer h-BN sheet including the edge. This bilayer configuration can be repeated along the out-of-plane direction to form a bulk N-edge. The total energies of the FM state and the AFM state (denoted AFM↑↓) for the bilayer and bulk N-edge are listed in Table I. The FM state remains the ground state and is preferred to the AFM↑↓ state by a similar difference in energy, compared to that of the monolayer h-BN. If the consecutive layers are each ferromagnetic but spin-polarized in the opposite direction with respect to each other (denoted AFM$^\uparrow_\downarrow$), the total energy is slightly higher than the FM case. All of these results reinforce our finding that the neighboring layers are electronically and magnetically largely independent from each other.

In Figure 3, the details of the atomic and magnetic configuration of the bilayer and bulk AB1-h-BN N-edge are presented. In Figure 3(a), the isosurface plots for magnetization (isovalue $n_\uparrow - n_\downarrow = \pm 0.02 \; |e|/a_0^3$) for the two AFM configurations of the bilayer edge are displayed (AFM$^{\uparrow\downarrow}_{\uparrow\downarrow}$=AFM↑↓ and AFM$^{\uparrow\uparrow}_{\downarrow\downarrow}$=AFM$^\uparrow_\downarrow$). In Figure 3(b,c,d), the DOS plots show that the bilayer FM edge is a half-metal, the bilayer AFM↑↓ state is a semiconductor, the bilayer AFM$^\uparrow_\downarrow$ state is a half-

		NM	FM	AFM↑↓	AFM$^\uparrow_\downarrow$
Monolayer	ΔE (meV)	$\equiv 0$	-218	-184	N/A
	E_{gap} (eV)	metal	half-metal	0.51	
Bilayer (AB)	ΔE	$\equiv 0$	-224	-187	-222
	E_{gap}	metal	half-metal	0.42	0.18
Bulk (AB)	ΔE	$\equiv 0$	-226	-195	-207
	E_{gap}	metal	half-metal	0.31	metal

Table I. Total energies and electronic band gaps of the nonmagnetic (NM), ferromagnetic (FM) and antiferromagnetic (AFM) configurations of the N-terminated zigzag edge of h-BN. Total energies are given per edge N atom.

semiconductor, and the bulk AFM$^\uparrow_\downarrow$ state is a metal. The bilayer AFM$^\uparrow_\downarrow$ state is similar to a bipolar magnetic semiconductor in which the valence band maximum (VBM) and the conduction band minimum (CBM) of one spin channel are at a higher energy than the those of the other spin channel [45, 46]. Here, the VBMs of the two spin channels are aligned but the CBMs are not aligned, leading to unequal gaps in the two spin channels, which, in the case of slight electron doping, would give rise to a spin-polarized edge current that would also be spatially confined to the top layer. Manipulating spins in semiconductors (semiconductor spintronics) is a rapidly developing field with promising applications in quantum computing [40, 42].

Because the energy differences between the FM and AFM configurations are low, thermodynamic considerations are needed to determine the expected configurations at a given temperature. Because spin polarization is localized to each edge N atom, we can use a discrete lattice model with interactions between neighbors instead of an itinerant spin model. In order to extract the interaction strengths, we have computed the energies of 10 single-layer, 5 bilayer and 5 bulk spin configurations. Because of the high precision required from these calculations, only the supercells compatible with the 12×1 k-point grid are considered, which are 1×1, 2×1, 3×1, 4×1 and 6×1. The spin configurations, total energies and the electronic gaps of these systems are listed in Table S1 of the Supplemental Material. These calculations have allowed us to extract the in-plane interaction energies for nearest, next-nearest and next-next-nearest neighbors (J_1, J_2 and J_3, respectively), as well as the out-of-plane interaction energy (J_4). The schematic representations of these interactions are presented in Figure S1, and the fitted values with the 90% confidence intervals are listed in Table S2 of the Supplemental Material. We find that zero is within the confidence interval for J_3 and J_4, meaning
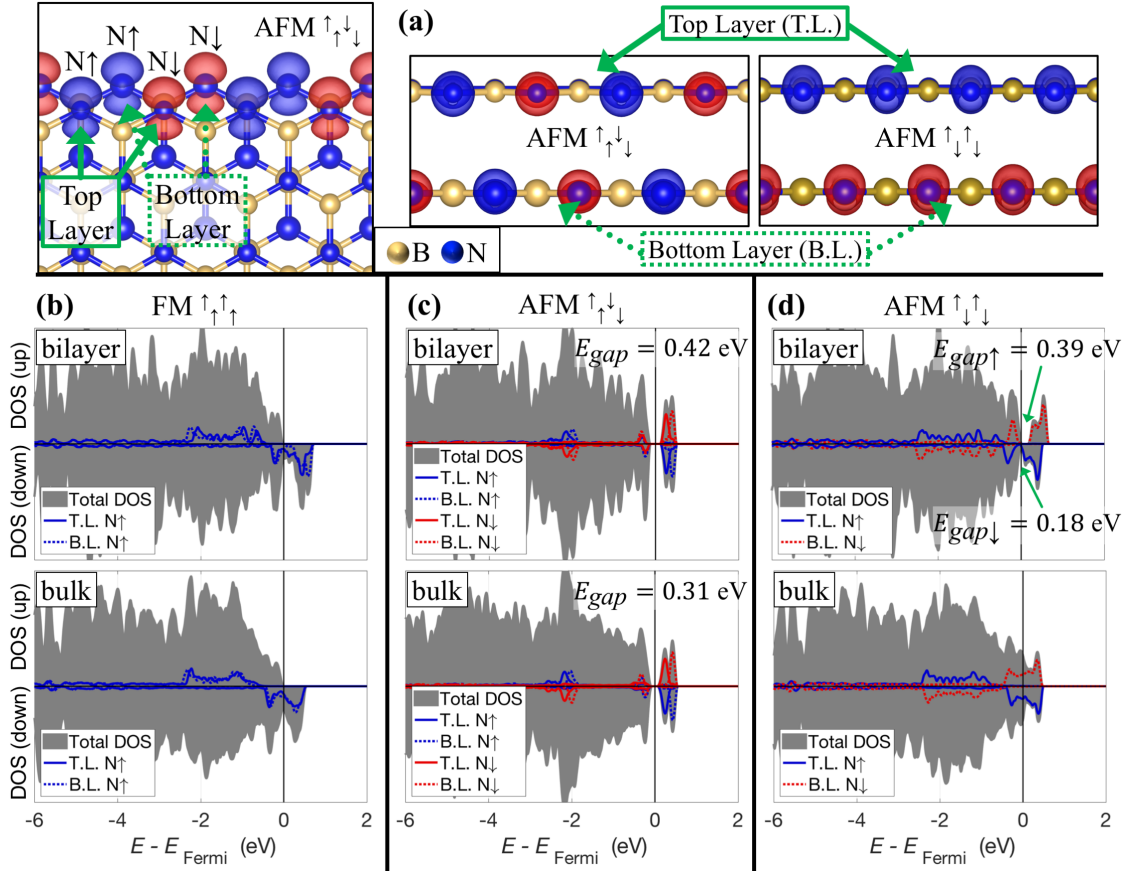
Figure 3. Atomic and electronic structure of the bilayer N-edge in AB-*h*-BN. (a) The isosurface plots for magnetization with the isovalue $n_\uparrow - n_\downarrow = \pm 0.02\ |e|/a_0^3$ are included in the atomic structure pictures for the two antiferromagnetic (AFM) configurations. (b) The spin-resolved densities-of-states plots including the projections onto the orbitals of the edge nitrogen atoms for the ferromagnetic (FM) configuration. (c, d) Same as (b), but for the two AFM configurations. The values of the electronic gaps, where they exist, are also printed on each panel.

that the open N-edge of each layer can be thought of as an independent one-dimensional spin chain with nearest and next-nearest neighbor interactions with the Hamiltonian:

$$H = J_1 \sum_i \boldsymbol{S_i} \cdot \boldsymbol{S_{i+1}} + J_2 \sum_i \boldsymbol{S_i} \cdot \boldsymbol{S_{i+2}} - \mu_\mathrm{B} H \sum_i S_i^z, \quad (1)$$

where $\boldsymbol{S_i}$ is a unit vector with x, y, z components that represents the spin at a lattice site i, $J_1 = -17$ meV is the nearest neighbor interaction energy, $J_2 = -12$ meV is the next-nearest neighbor interaction energy, μ_B is the Bohr magneton, and H is the external magnetic field. Because spin–orbit interaction in *h*-BN is extremely weak [47] (two or three orders of magnitude smaller than J_1 and J_2), we do not expect magnetic anisotropy in this system above ~ 10 K [48]. As a result of this lack of anisotropy, there is no easy axis present in this system which leads to a continuous spin model (Heisenberg) instead of a discrete spin model (Ising); furthermore, the external magnetic field can be assumed to apply in the z-direction without loss of generality.

This model corresponds to classical one-dimensional isotropic Heisenberg model with nearest and next-nearest neighbor interactions. For such a model, according to the Mermin–Wagner theorem, in the absence of an external magnetic field, the ferroelectric ground state is not stable for any temperature greater than absolute zero [49]. Although an exact analytical solution to this model is not known, when both J_1 and J_2 are negative, *i.e.* both the interactions are ferromagnetic, its behavior is analogous to the Heisenberg model with only nearest-neighbor interactions [50, 51] whose exact solution is known [52]. In order to determine the behavior of the expected value of spin ($\langle S_z \rangle$) and the spin pair correlation function (ξ_z) in our system where J_1 and J_2 have specific numerical values, we have conducted a Monte Carlo study a modified version of the Metropolis algorithm [53]. In the usual Metropolis algorithm for the Heisenberg model, at each simulation step, an attempt is made to randomize one of the spins [54]. However, this leads to a critical slowing down where the decorrelation time diverges near the crit-

ical temperature [55, 56], which in this case is 0 K. To overcome this problem to some degree, instead of choosing the proposed direction of the spin at random, we choose it according to the formula

$$\Delta\theta = \cos^{-1}\left(K^{-1}\log(\exp(-K) + 2r\sinh(K))\right), \quad (2)$$

where $\Delta\theta$ is the angle between the new spin and the old spin, $K = {}^{(J_1+J_2)}\!/_{(k_BT)}$ and r is a random number between 0 and 1 [57]. This attempt is then accepted or rejected based on the Boltzmann factor of the energy difference between the proposed and original configurations, which generates a sampling of the configuration space that obeys the detailed balance condition [56].

We have obtained a collection of results by running these simulations with free boundary conditions where the number of spins is chosen between $N = 20$ and $N = 200$ to be at least a few times the spin pair correlation length, the temperature varies between $T = 12$ K and $T = 232$ K and the external magnetic field varies between $H = 0$ T and $H = 100$ T. As an example, the correlation functions and the evolution of the average site energy for a simulation for $H = 0.1$ T and $T = 70$ K are presented in Figures S2, S3 and S4 of the Supplemental Material. $\langle S_z \rangle$ and ξ_z for all temperatures and magnetic fields are plotted in Figure 4. The error bars are obtained from the standard deviations over ten simulations conducted for each H, T pair. According to our results on $\langle S_z \rangle$ [Figure 4(a)], it is possible to magnetize significantly these edges with external fields of 4 T and above. This is higher than the field for magnetic saturation (about 1 T) found in an experiment [44]. However, in this experiment, the observed magnetization may have originated from not only edges but also other defects such as vacancies and pores, which are also known to have magnetic properties [29]. Although the average spin for $H = 0$ T is zero for all nonzero temperatures, the spin pair correlation length is not zero [Figure 4(b)] and increases exponentially as T approaches zero. As a result, the expectation value of the site energy decreases as $T \to 0$ [Figure S5 of the Supplemental Material]. At low-temperature experiments (liquid N_2 temperatures or lower), correlation lengths comparable to the edge length may produce an enhanced magnetization in the presence of small and intermediate-sized nanopores. The heat capacity (C_v) and magnetic susceptibility (χ) of this system for all H, T pairs are also presented in Figures S6 and S7 of the Supplemental Material, whose behaviors are analogous to similar models [58]. Experiments that can isolate the magnetic behavior of edges in h-BN sheets, such as electron energy loss spectroscopy (EELS) [30] and scanning tunneling microscopy (STM) [59] are needed to test these findings. The ability to induce the ferromagnetic state at the edge *via* an external field, which is also the state with less electrical resistance (Figure 2), indicates the potential for magnetoresistive effect [36, 37, 39]. Furthermore, if edges could be stacked so that FM and
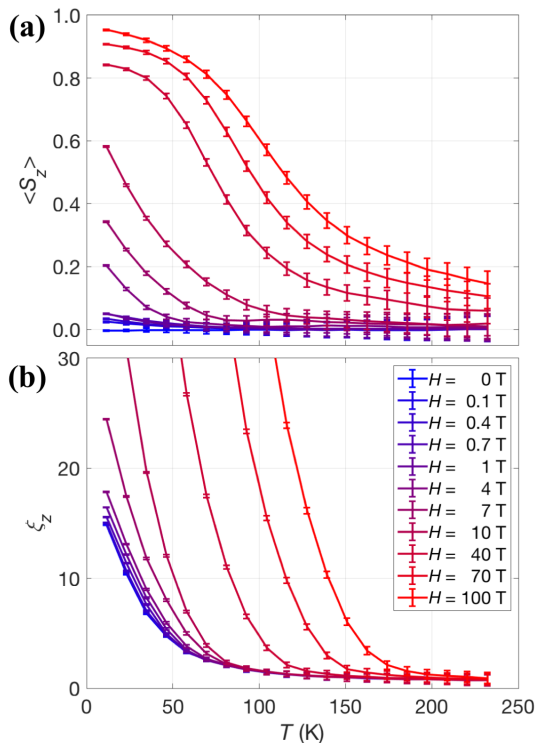

Figure 4. The expected value of spin ($\langle S_z \rangle$) (a) and spin pair correlation function (ξ_z) (b) for all temperatures and magnetic fields. The error bars are obtained from the standard deviations over ten simulations conducted for each H, T pair.

AFM edges alternate, giant magnetoresistance may be observed [36, 37, 39].

B. Closed Edges in h-BN

We now turn to other possibilities of bilayer edge reconstructions in h-BN which result in "closed" edges. First, as reference, we compute the relaxation of the N-edge in AA- and AA$'$-h-BN. In AA-h-BN, edge N atoms in neighboring layers are directly aligned, and relax out-of-plane to form an sp^2 type bond [Figure 5(a,b)]. The degree of out-of-plane relaxation is quite large, where the highest interlayer distance becomes 6.66 Å. In AA$'$-h-BN, due to the inequivalence between the neighboring layers, an N-edge in the bottom layer must align with a B-edge in the top layer. These edges form an interlayer bond which creates a structure that can be understood as a half BN nanotube [Figure 5(d,e)]. Our findings on the closed AA$'$-h-BN edge agrees with previous calculations and observations [30]. In both of these edge reconstructions, each atom makes three bonds, which eliminates unpaired electrons and results in nonmagnetic insulators [Figure 5(c,f)].
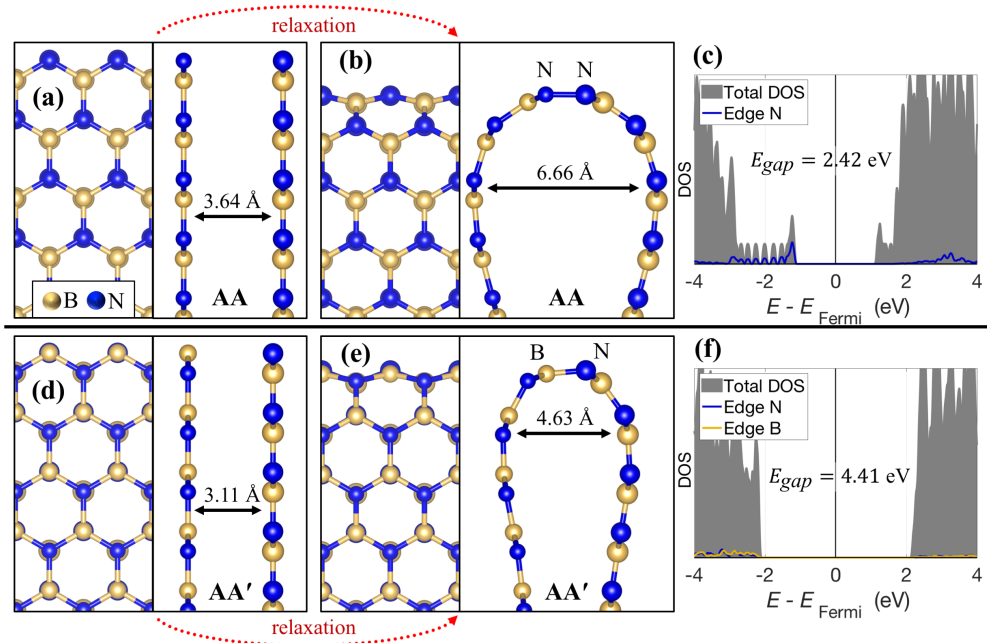
In the case of AB-h-BN, the starting configuration of

Figure 5. Edge reconstructions of AA- and AA′-h-BN. Top and side views of the atomic structure before and after the relaxation is presented for AA-h-BN (a,b) and AA′-h-BN (d,e). The densities-of-states plots including the projections onto the orbitals of the edge atoms marked in the middle panels are presented for AA-h-BN (c) and AA′-h-BN (f).

the bilayer N-edge can be created in two different ways by terminating the layers at different N rows. The first is presented in Figure 6(a). When the atoms are allowed to relax, no interlayer bonds form, leading to the open edge structure [Figure 6(b,c)] which we have discussed above. This bilayer edge is the one we were able to identify in the HRTEM study [29]. However, it is conceivable that while the edges form, the B atom bonded to the edge N atom in the top layer finds the edge N atom in the bottom layer and forms a bridge between the two edges. This reconstruction is shown in Figure 6(d). This highly distorted 2×1 edge structure has not been observed, but may arise under different experimental conditions. Because each atom makes three bonds, eliminating unpaired electrons, the DOS plot shows a nonmagnetic insulator [Figure 6(e)].

The second way of creating a starting configuration for bilayer N-edge in AB-h-BN is presented in Figure 7(a). When the atoms are allowed to relax, large out-of-plane relaxations occur, leading to the closed edge structure shown in Figure 7(b). The large out-of-plane relaxations are accompanied by a significant in-plane contraction perpendicular to the edge, which was not observed in the HRTEM study [29]. It is possible that while the edges form, the B atom bonded to the edge N atom in the bottom layer finds the edge N atom in the top layer and forms a bridge between the two edges. This reconstruction is shown in Figure 7(d). Although this forms a closed edge with a 2×1 reconstruction, the in-plane re-

laxations are strictly confined to the edge atoms and no significant contraction perpendicular to the edge is observed. As a result, this structure would be very difficult to identify in an HRTEM study such as Ref. 29, and therefore is not ruled out. In both of these reconstructions, because each atom makes three bonds, eliminating unpaired electrons, the DOS plots reveal nonmagnetic insulators [Figure 7(c,e)].

We note that in this study we have focused on stacking types with a periodicity of two layers, such as AA′ and AB, although the ABC stacking in h-BN has also been observed, which results in a rhombohedral lattice structure [9]. ABC stacking is obtained by applying one of the lateral shifts shown in Figure 1(c,d) consecutively to each layer, which results in a structure that repeats every three layers. Therefore, a bilayer film from ABC-h-BN is equivalent to bilayer AB-h-BN, which we have covered. For thicker multilayer edges, the termination of each neighboring layer pair could be either as in Figure 6(a) or as in Figure 7(a). The simplest multilayer edge structure in ABC-h-BN would be where each layer pair terminates as in Figure 6(a) and relaxes into the open edge structure [Figure 6(b)]. Because in this case each layer is essentially decoupled from others, we would expect this structure to be electronically and magnetically equivalent to the multilayer AB-h-BN open edge structure. However, because other combinations of edge terminations are also possible, multilayer edges in ABC-h-BN can be more complicated, potentially deserving a
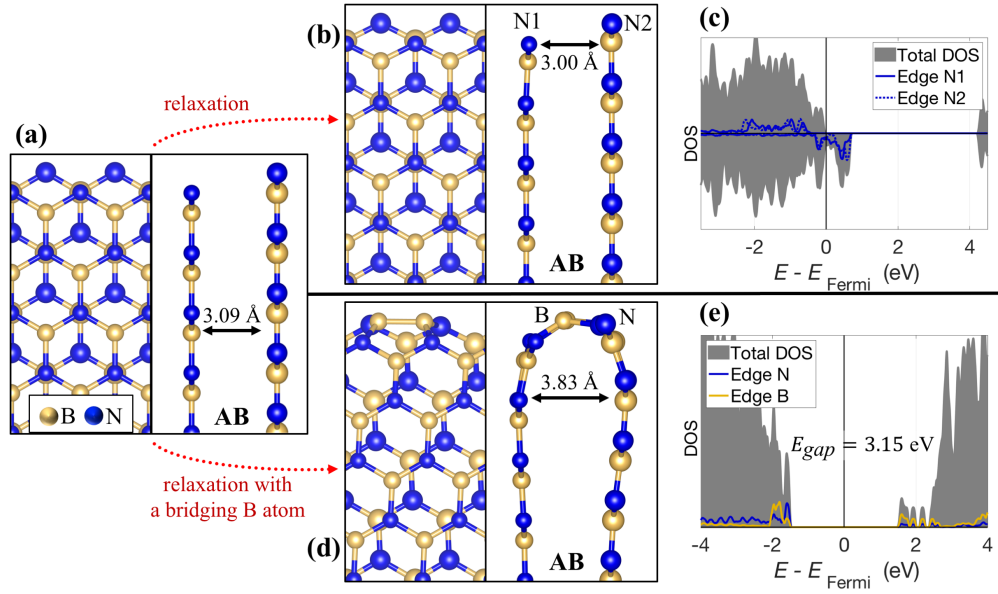
Figure 6. Edge reconstructions of AB-h-BN arising from the first starting configuration. Top and side views of the atomic structure before (a) and after the relaxation (b) are presented, along with the spin-resolved densities-of-states plot (c) including the projections onto the orbitals of the edge atoms marked in the middle panel. The structure that results from adding a bridging B atom between the two edges is presented in (d) along with its densities-of-states plot (e) including the projections onto the orbitals of the edge atoms marked in the middle panel.
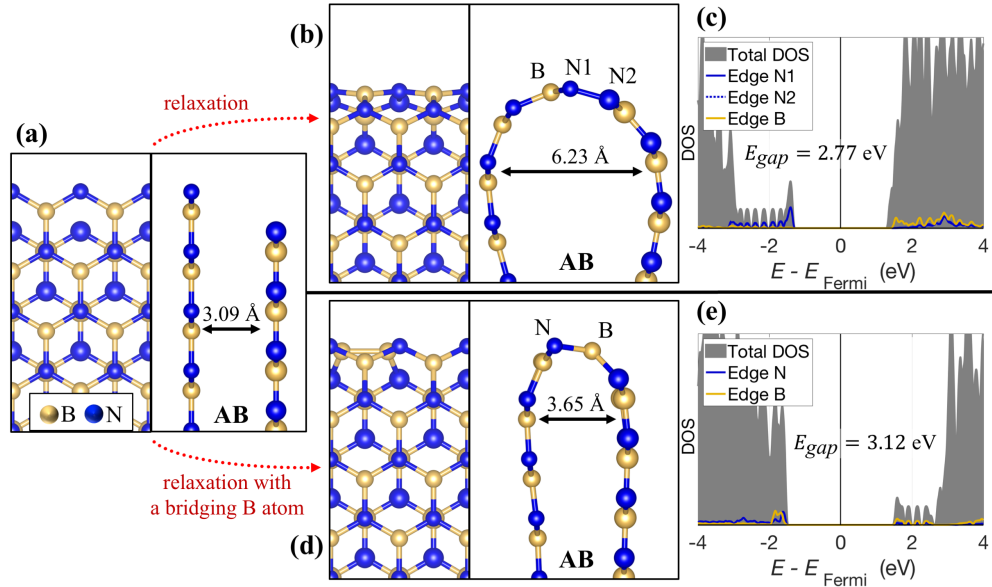

Figure 7. Edge reconstructions of AB-h-BN arising from the second starting configuration. Top and side views of the atomic structure before (a) and after the relaxation (b) are presented, along with the densities-of-states plot (c) including the projections onto the orbitals of the edge atoms marked in the middle panel. The structure that results from adding a bridging B atom between the two edges is presented in (d) along with its densities-of-states plot (e) including the projections onto the orbitals of the edge atoms marked in the middle panel.

		NM	FM	AFM↑↓
AA	ΔE (meV)	≡ 0	−164	−85
	E_{gap}(eV)	metal	0.15	0.31
AA′	ΔE	≡ 0	−197	−152
	E_{gap}	metal	0.12	0.43
AB1	ΔE	≡ 0	−180	−115
	E_{gap}	metal	0.18	0.33
AB2	ΔE	≡ 0	−206	−163
	E_{gap}	metal	0.13	0.47

Table II. Total energies and electronic band gaps of the non-magnetic (NM), ferromagnetic (FM) and antiferromagnetic (AFM) configurations of the N-terminated step edge of h-BN in AA, AA′ and AB stacking sequences. Total energies are given per edge N atom.

dedicated separate study.

C.   Step Edges in h-BN

In real h-BN sheets, it is difficult to manufacture bi-layer edges that are aligned to form a collection of stacked open N-edges as in Figure 6(b) although a preference for such alignment has been observed in our study where edges were fabricated through a high-energy electron beam [29]. Thus, it is important to investigate the behavior of a monolayer edge when its neighbor does not also have an edge nearby. To this end, we have investigated the behavior of step edges in h-BN for AA, AA′ and AB stacking sequences. We have found that the monolayer edges remain intact and can be in an FM or AFM state. In Table II, we summarize these findings. We observe that the energy difference between the FM and AFM states depends on the stacking sequence, and hence the interaction energies in equation (1) for each edge would be different. However, the FM state remains the ground state and the AFM state is higher in energy by similar amounts, thus the resulting models are not expected to be qualitatively different. Therefore, the N-edge in a single layer should remain magnetically active when it is sandwiched by other sheets that do not have an edge in the immediate vicinity, regardless of the stacking sequence.

In Figure 8, we present the atomic and electronic structures of the four step edges we have investigated. We find that the ground state electronic structure of all four step edges is a FM half-semiconductor with band gaps in the infrared region $(0.12 - 0.18$ eV$)$, and the AFM state is a

nonmagnetic semiconductor with band gaps also in the infrared region $(0.31 - 0.47$ eV$)$. Our findings indicate that step edges can be utilized to stabilize a magnetic edge in AA′-h-BN. We also find that the amount of bending of the step edge toward the full sheet is significantly different between the AB1 and AB2 stacking sequences $(0.23$ Å and 0.06 Å, respectively), due to the alignment of the edge N atom in the top layer with a B atom *vs.* a hollow site in the bottom layer.

IV.   CONCLUSION

We conducted a first-principles study of the commonly observed nitrogen-terminated zigzag edges (N-edges) in h-BN, with a focus on Bernal-stacked h-BN (AB-h-BN). We showed that the N-edges in the monolayer h-BN possess various spin configurations that are within a small total energy window. Because the magnetization is localized in the vicinity of each N atom, we constructed a discrete lattice model for magnetism on the edge, which yields nm-scale correlation lengths at temperatures in the $10 - 50$ K range. Although in the long edge limit $(N \to \infty)$ no significant magnetization is expected in external magnetic fields less than 1 Tesla, the shorter edges that lie in the vertices of nanopores may exhibit significant magnetization that may be probed by EELS or STM experiments. We showed that these edges remain open in AB-h-BN and can be stacked in the out-of-plane direction to form bilayer or multilayer edges, where the spins in neighboring layers do not interact significantly. If, as we proposed, the spins in multilayer AB-h-BN can be manipulated *via* magnetic fields, magnetoresistive effects as well as spintronic applications may be achieved in these reduced-dimensional systems. We also discussed the possibilities of closed edge reconstructions in AB-h-BN, as well as in AA′-h-BN where they inevitably occur. Finally, we examined step edges in h-BN with various stacking sequences, which indicates that the edges in a single layer are stable in all stacking sequences when they are capped by full sheets. We hope that our results motivate experimental studies that closely investigate the magnetic and electronic properties of these edges in h-BN.
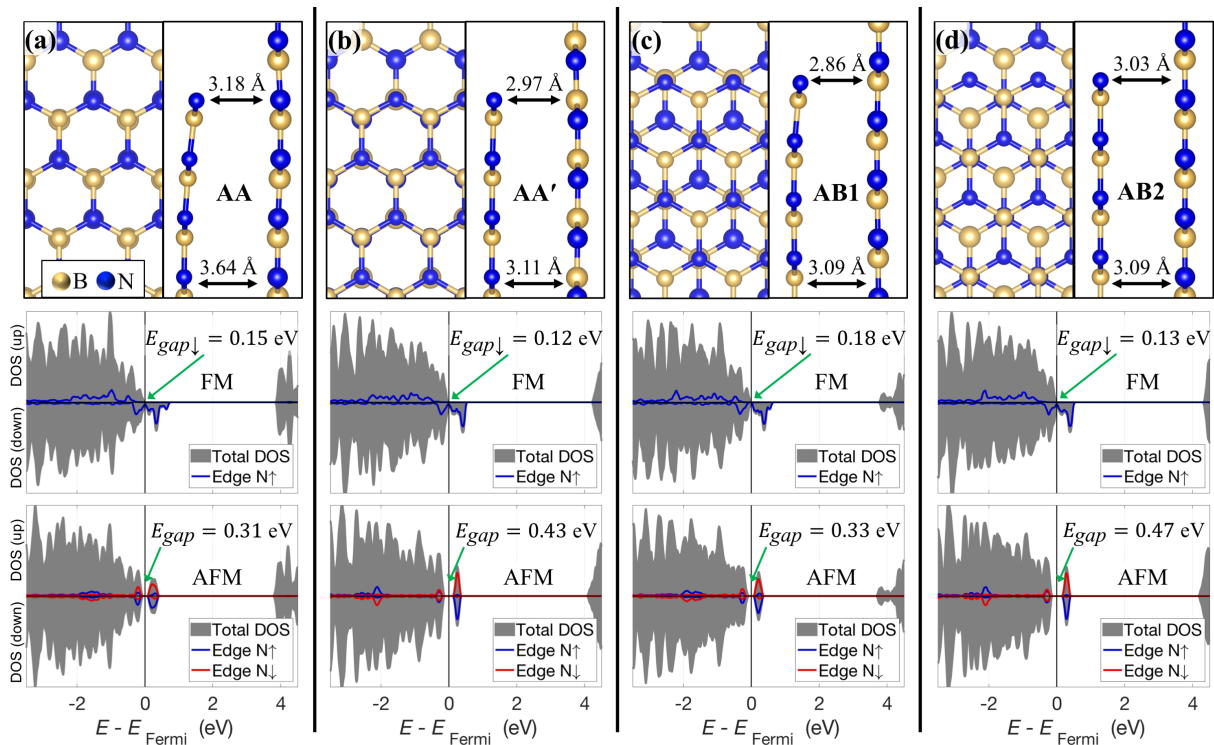
Figure 8. Atomic and electronic structures of the step edges in the AA (a), AA′ (b), AB1 (c) and AB2 (d) stacking sequences. For each case, the spin-resolved densities-of-states plots including the projections onto the orbitals of the edge nitrogen atoms are presented for both the FM and AFM states. The values of the electronic gaps, where they exist, are also printed on each panel.

[1] A. Celis, M. N. Nair, A. Taleb-Ibrahimi, E. H. Conrad, C. Berger, W. A. d. Heer, and A. Tejeda, Journal of Physics D: Applied Physics 49, 143001 (2016), publisher: IOP Publishing.

[2] S. P. Koenig, L. Wang, J. Pellegrino, and J. S. Bunch, Nature Nanotechnology 7, 728 (2012).

[3] S. Choi, T. T. Tran, C. Elbadawi, C. Lobo, X. Wang, S. Juodkazis, G. Seniutinas, M. Toth, and I. Aharonovich, ACS Applied Materials & Interfaces 8, 29642 (2016).

[4] J. Zhao, G. He, S. Huang, L. F. Villalobos, M. Dakhchoune, H. Bassas, and K. V. Agrawal, Science Advances 5, eaav1851 (2019).

[5] J. D. Caldwell, I. Aharonovich, G. Cassabois, J. H. Edgar, B. Gil, and D. N. Basov, Nature Reviews Materials 4, 552 (2019), number: 8 Publisher: Nature Publishing Group.

[6] Y. Qi and L. G. Hector, Applied Physics Letters 90, 081922 (2007).

[7] N. Marom, J. Bernstein, J. Garel, A. Tkatchenko, E. Joselevich, L. Kronik, and O. Hod, Physical Review Letters 105, 046801 (2010).

[8] G. Constantinescu, A. Kuc, and T. Heine, Physical Review Letters 111, 036104 (2013).

[9] S. M. Gilbert, T. Pham, M. Dogan, S. Oh, B. Shevitski, G. Schumm, S. Liu, P. Ercius, S. Aloni, M. L. Cohen, and A. Zettl, 2D Materials 6, 021006 (2019).

[10] N. Alem, R. Erni, C. Kisielowski, M. D. Rossell, W. Gannett, and A. Zettl, Physical Review B 80, 155425 (2009).

[11] J. H. Warner, M. H. Rümmeli, A. Bachmatiuk, and B. Büchner, ACS Nano 4, 1299 (2010).

[12] M. H. Khan, G. Casillas, D. R. G. Mitchell, H. K. Liu, L. Jiang, and Z. Huang, Nanoscale 8, 15926 (2016).

[13] Y. Ji, B. Calderon, Y. Han, P. Cueva, N. R. Jungwirth, H. A. Alsalman, J. Hwang, G. D. Fuchs, D. A. Muller, and M. G. Spencer, ACS Nano 11, 12057 (2017).

[14] V. Barone and J. E. Peralta, Nano Letters 8, 2210 (2008).

[15] L. Lai, J. Lu, L. Wang, G. Luo, J. Zhou, R. Qin, Z. Gao, and W. N. Mei, The Journal of Physical Chemistry C 113, 2273 (2009).

[16] R. Mukherjee and S. Bhowmick, Journal of Chemical Theory and Computation 7, 720 (2011).

[17] S. S. Yamijala and S. K. Pati, The Journal of Physical Chemistry C 117, 3580 (2013).

[18] J. Deng, Y. Yin, H. Niu, X. Ding, J. Sun, and N. V. Medhekar, Scientific Reports 7, 1 (2017).

[19] A. Zobelli, A. Gloter, C. P. Ewels, G. Seifert, and C. Colliex, Physical Review B **75**, 245402 (2007).

[20] J. C. Meyer, A. Chuvilin, G. Algara-Siller, J. Biskupek, and U. Kaiser, Nano Letters **9**, 2683 (2009).

[21] J. Kotakoski, C. H. Jin, O. Lehtinen, K. Suenaga, and A. V. Krasheninnikov, Physical Review B **82**, 113404 (2010).

[22] J. S. Kim, K. B. Borisenko, V. Nicolosi, and A. I. Kirkland, ACS Nano **5**, 3977 (2011), publisher: American Chemical Society.

[23] G. H. Ryu, H. J. Park, J. Ryou, J. Park, J. Lee, G. Kim, H. S. Shin, C. W. Bielawski, R. S. Ruoff, S. Hong, and Z. Lee, Nanoscale **7**, 10600 (2015).

[24] A. G. Rajan, K. S. Silmore, J. Swett, A. W. Robertson, J. H. Warner, D. Blankschtein, and M. S. Strano, Nature Materials **18**, 129 (2019), number: 2 Publisher: Nature Publishing Group.

[25] O. Mouhoub, R. Martinez-Gordillo, J. Nelayah, G. Wang, J.-H. Park, K. K. Kim, Y. H. Lee, C. Bichara, A. Loiseau, C. Ricolleau, H. Amara, and D. Alloyeau, Physical Review Materials **4**, 014005 (2020), publisher: American Physical Society.

[26] N. Alem, R. Erni, C. Kisielowski, M. D. Rossell, P. Hartel, B. Jiang, W. Gannett, and A. Zettl, Physica Status Solidi – Rapid Research Letters **5**, 295 (2011).

[27] T. Pham, A. L. Gibb, Z. Li, S. M. Gilbert, C. Song, S. G. Louie, and A. Zettl, Nano Letters **16**, 7142 (2016).

[28] S. M. Gilbert, G. Dunn, A. Azizi, T. Pham, B. Shevitski, E. Dimitrov, S. Liu, S. Aloni, and A. Zettl, Scientific Reports **7**, 15096 (2017).

[29] M. Dogan, S. M. Gilbert, T. Pham, B. Shevitski, P. Ercius, S. Aloni, A. Zettl, and M. L. Cohen, Applied Physics Letters **117**, 023102 (2020), publisher: AIP Publishing LLC AIP Publishing.

[30] N. Alem, Q. M. Ramasse, C. R. Seabourne, O. V. Yazyev, K. Erickson, M. C. Sarahan, C. Kisielowski, A. J. Scott, S. G. Louie, and A. Zettl, Physical Review Letters **109**, 205502 (2012).

[31] J. P. Perdew and A. Zunger, Physical Review B **23**, 5048 (1981).

[32] P. Giannozzi, S. Baroni, N. Bonini, M. Calandra, R. Car, C. Cavazzoni, Davide Ceresoli, G. L. Chiarotti, M. Cococcioni, I. Dabo, A. D. Corso, S. d. Gironcoli, S. Fabris, G. Fratesi, R. Gebauer, U. Gerstmann, C. Gougoussis, Anton Kokalj, M. Lazzeri, L. Martin-Samos, N. Marzari, F. Mauri, R. Mazzarello, Stefano Paolini, A. Pasquarello, L. Paulatto, C. Sbraccia, S. Scandolo, G. Sclauzero, A. P. Seitsonen, A. Smogunov, P. Umari, and R. M. Wentzcovitch, Journal of Physics: Condensed Matter **21**, 395502 (2009).

[33] D. R. Hamann, Physical Review B **88**, 085117 (2013).

[34] M. L. Cohen, M. Schlüter, J. R. Chelikowsky, and S. G. Louie, Physical Review B **12**, 5575 (1975).

[35] S. Grimme, Journal of Computational Chemistry **27**, 1787 (2006).

[36] G. A. Prinz, Science **282**, 1660 (1998), publisher: American Association for the Advancement of Science Section: Review.

[37] S. A. Wolf, D. D. Awschalom, R. A. Buhrman, J. M. Daughton, S. v. Molnár, M. L. Roukes, A. Y. Chtchelkanova, and D. M. Treger, Science **294**, 1488 (2001), publisher: American Association for the Advancement of Science Section: Special Reviews.

[38] I. Žutić, J. Fabian, and S. Das Sarma, Reviews of Modern Physics **76**, 323 (2004), publisher: American Physical Society.

[39] C. Felser, G. H. Fecher, and B. Balke, Angewandte Chemie International Edition **46**, 668 (2007).

[40] D. D. Awschalom and M. E. Flatté, Nature Physics **3**, 153 (2007), number: 3 Publisher: Nature Publishing Group.

[41] O. V. Yazyev, Reports on Progress in Physics **73**, 056501 (2010), publisher: IOP Publishing.

[42] D. D. Awschalom, L. C. Bassett, A. S. Dzurak, E. L. Hu, and J. R. Petta, Science **339**, 1174 (2013), publisher: American Association for the Advancement of Science Section: Review.

[43] A. Du, Y. Chen, Z. Zhu, R. Amal, G. Q. M. Lu, and S. C. Smith, Journal of the American Chemical Society **131**, 17354 (2009).

[44] M. S. Si, D. Gao, D. Yang, Y. Peng, Z. Y. Zhang, D. Xue, Y. Liu, X. Deng, and G. P. Zhang, The Journal of Chemical Physics **140**, 204701 (2014).

[45] X. Li, X. Wu, Z. Li, J. Yang, and J. G. Hou, Nanoscale **4**, 5680 (2012).

[46] X. Li and J. Yang, National Science Review **3**, 365 (2016).

[47] K. Zollner, M. Gmitra, and J. Fabian, Physical Review B **99**, 125151 (2019), publisher: American Physical Society.

[48] O. V. Yazyev and M. I. Katsnelson, Physical Review Letters **100**, 047209 (2008).

[49] N. D. Mermin and H. Wagner, Physical Review Letters **17**, 1133 (1966).

[50] C. K. Majumdar and D. K. Ghosh, Journal of Mathematical Physics **10**, 1388 (1969), publisher: American Institute of Physics.

[51] C. K. Majumdar and D. K. Ghosh, Journal of Mathematical Physics **10**, 1399 (1969), publisher: American Institute of Physics.

[52] M. E. Fisher, American Journal of Physics **32**, 343 (1964).

[53] N. Metropolis, A. W. Rosenbluth, M. N. Rosenbluth, and A. H. Teller, The Journal of Chemical Physics **21**, 1087 (1953).

[54] Z. Slanic, H. Gould, and J. Tobochnik, Computers in Physics **5**, 630 (1991), publisher: American Institute of Physics.

[55] G. T. Barkema and M. E. J. Newman, arXiv:cond-mat/9703179 (1997), arXiv: cond-mat/9703179.

[56] M. Dogan and S. Ismail-Beigi, The Journal of Physical Chemistry C **123**, 14350 (2019).

[57] N. A. Lurie, D. L. Huber, and M. Blume, Physical Review B **9**, 2171 (1974), publisher: American Physical Society.

[58] J. C. Bonner, Journal of Applied Physics **49**, 1299 (1978), publisher: American Institute of Physics.

[59] D. Wong, J. Velasco Jr, L. Ju, J. Lee, S. Kahn, H.-Z. Tsai, C. Germany, T. Taniguchi, K. Watanabe, A. Zettl, F. Wang, and M. F. Crommie, Nature Nanotechnology **10**, 949 (2015).